Supporting Information for:

Micro/nanosized Untraditional Evaporated Structures Based on Closely Packed Monolayer Binary Colloidal Crystals and Their Fine Structure Enhanced Properties

Junfeng Zheng,[† #] Zhigao Dai,[† #] Fei Mei,[†,‡] Xiangheng Xiao,[†,§ *] Lei Liao,[†] Wei Wu,[†] Xinyue Zhao,[†] Jianjian Ying,[†] Feng Ren,[†] and Changzhong Jiang[† *]

[†] Department of Physics, Hubei Nuclear Solid Physics Key Laboratory and Center for Ion Beam Application, Wuhan University, Wuhan 430072, China

[‡] School of Electrical & Electronic Engineering, Hubei University of Technology, Wuhan 430068, P. R. China

[§] Department of Chemistry and Biochemistry, University of California, Los Angeles, California 90095, USA

Supporting Information

(1) The defect percentage of different bCCs patterns.

(2) LS_2 patterns with different T_D.

(3) Three different levels of disordered bCCs due to the corresponding noncompact monolayer.

(4) LS_2 and LS_6 patterns with 30 min oxygen plasma treatment and Ag nanoarrays based on them.

(1) The defect percentage of different bCCs patterns:

The defect percentage in the binary monolayer crystal patterns is evaluated statistically, and the detail has been shown in Chart S1.

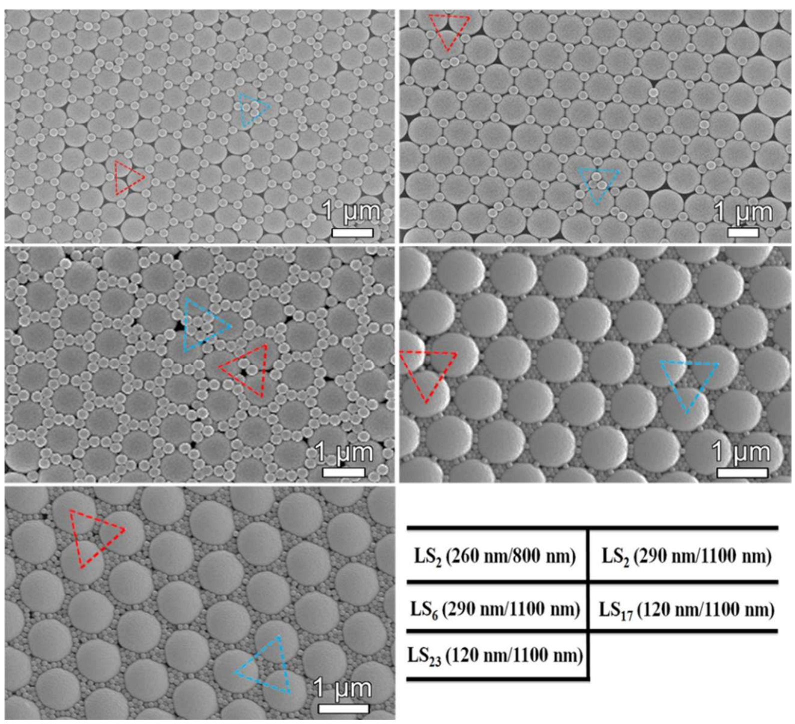

Figure S1. SEM images of the monolayer bCCs with four patterns. Two types of different defects are shown in blue triangle and red triangle. The red triangle shows that the number of small spheres occupied triangular voids is less than required. And the

blue triangle shows that the number of small spheres occupied triangular voids is more than required.

Chart S1. The statistics of different defects in bCCs patterns corresponding to Figure S1.

pattern	defect			defect percentage
	red triangle	blue triangle	summation	
LS_2 (260 nm/800 nm)	48	34	82	26%(82/314)
LS_2 (290 nm/1100 nm)	34	15	49	26% (49/184)
LS_6 (290 nm/1100 nm)	14	11	25	23% (25/108)
LS_{17} (120 nm/1100 nm)	4	4	8	9% (8/85)
LS_{23} (120 nm/1100 nm)	2	2	4	5%(4/75)

(2) LS_2 patterns with different T_R:

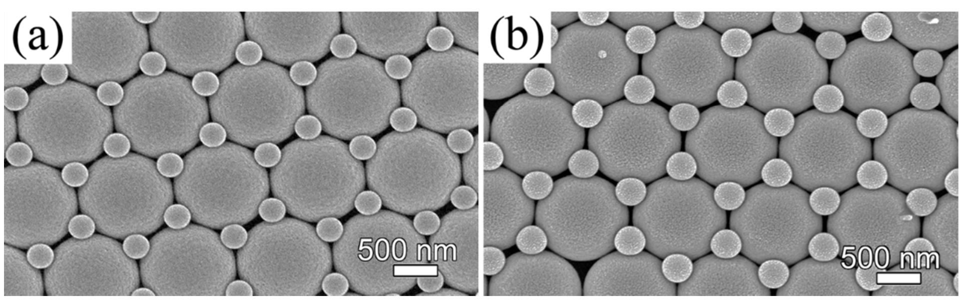

Figure S2. SEM images of monolayer colloidal crystals with single-sized spheres or different-sized spheres. (a) T_R=0.264 (290 nm and 1100 nm); (b) T_R=0.345 (380 nm and 1100 nm).

In Figure S2, changing T_R to the values of 0.264 and 0.345 (290 nm/1100 nm and 380 nm/1100 nm in this work) approaching to 0.325 (260 nm/800 nm), we can see the same ordered patterns LS_2, as illustrated in Figure 2e and Figure 2f respectively. Obviously, based on the close-packed structure composed of large spheres, high-quality LS_2 patterns with T_R value between 0.25 and 0.35 can be obtained reliably.

(3) Three different levels of disordered bCCs due to the corresponding noncompact monolayer:

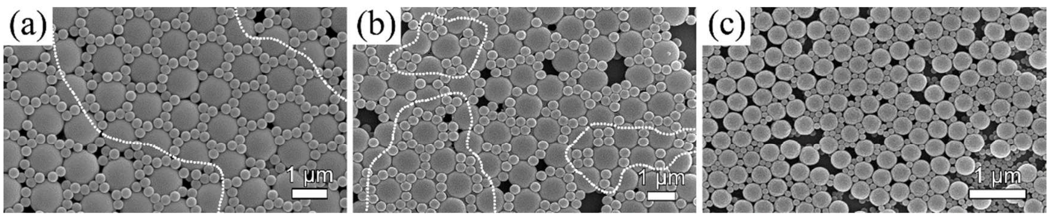

Figure S3. SEM images of three different levels of noncompact monolayer bCCs. (a) A few gaps in LS_6 (290 nm and 1100nm); (b) larger defect in monolayer with local ordered structure (360nm and 1100 nm); (c) the disorder monolayer (120nm and 360nm).

Three different levels of noncompact monolayer may be produced by self-assembly at water-air interface, as illustrated in Figure 5a-c. Here, under T_N =6, we keep T_R values be 0.264 (290 nm/1100 nm), 0.327 (360 nm/1100 nm), and 0.333 （120 nm/360 nm）in the three pictures respectively. Some interstitial volumes between large PS spheres have been increased, as representatively shown in Figure S3(a). In this view, local area of the monolayer is considerably in line with LS_6 pattern (see the dashed line in Figure S3(a)). Insufficiently disperse or mix the PS sphere suspensions may lead to the phenomenon existed in Figure S3(b). Due to the loose structure consisted of large spheres, more vacancies of the large PS spheres have been produced. Most of the small spheres occupy the interstitial sites and triangular voids, tending to form an orderly structure with two-spheres, three integrations, and four-spheres (see the dashed line in Figure S3(b). Otherwise, if alcohol in the colloidal suspension overdoses, phenomenon like Figure S3(b) will appear normally. In Figure S3(c), the disorder configuration with large-area defects resulted in unclose-packed large spheres. Compared with other views, spheres with smaller size in Figure S3(c) is sensitive that can hardly be controlled to form close-packed structures.

Due to the same size, large spheres can self-assemble into close-packed structure and easily assure the interstitial volume be consistent. In this case, making the large spheres closely packed is essential to fabricate bCCs. It is evident from Figure S3 that factors related to large spheres should be first considered to form closely packed monolayer. Furthermore, the preparation of appropriate binary colloidal suspension is an essential and challenging step.

(4) LS_2 and LS_6 patterns with 30 min oxygen plasma treatment and Ag nanoarrays based on them:

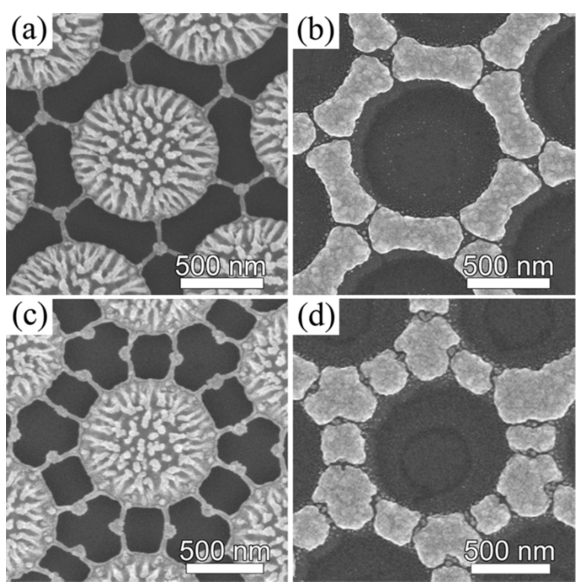

Figure S4. SEM images of the different etched bCCs patterns and Ag nanoarrays produced by them as colloidal lithography masks. (a) LS_2, 30 min; (b) Ag nanoarrays corresponding to

Figure S4(a); (c) LS_6, 30 min; (d) Ag nanoarrays corresponding to Figure S4(c).

Figure S4 shows the bCCs patterns with 30 min oxygen plasma treatment and Ag nanoarrays based on them. The gap size between the particles in Figure S4(b) and Figure S4(d) can be controlled to be smaller than 10 nm 15 nm respectively.